WILEY-VCH

Structural Color Materials with Color Mixing Effect Using Noble Metal-free Plasmonic Particles in SiO_2–ZrN System

*Shinji Noguchi, Milena Lama, Yuta Fujii, Akira Miura, Kiyoharu Tadanaga**

S. Noguchi
Graduate School of Chemical Sciences and Engineering, Hokkaido University, Kita-13, Nishi-8, Kita-ku, Sapporo 060-8628, Japan

M. Lama
Institute for Chemical Reaction Design and Discovery (WPI-ICReDD), Hokkaido University, Kita-21, Nishi-11, Kita-ku, Sapporo 001-0021, Japan

Y. Fujii, A. Miura, K. Tadanaga
Faculty of Engineering, Hokkaido University, Kita-13, Nishi-8, Kita-ku, Sapporo, 060-8628, Japan

*Corresponding author
E-mail: tadanaga@eng.hokudai.ac.jp

Keywords: core–shell particles, metal nitrides, plasmonics, photonics, structural color, self-assembly

Abstract

Structurally colored materials with a color mixing effect were developed using SiO_2–ZrN core–shell particles, where ZrN nanoparticles used as shells exhibited localized surface plasmon resonances (LSPRs). ZrN nanoparticles (10–30 nm) were attached to monodispersed SiO_2 particles by modifying SiO_2 particles with polymers. The attached ZrN nanoparticles exhibited a plasmon resonance absorption band at 700 nm. These SiO_2–ZrN core–shell particles have a highly monodisperse particle size and assemble into a particle-stacked film with Bragg diffraction light in the visible spectrum. The particle-stacked film of the SiO_2–ZrN core–shell particles exhibited the maximum reflection depending on the particle size of the SiO_2 core. The ratio of the reflection intensity in the long-wavelength region corresponding to the ZrN absorption to that in the short-wavelength region of the particle-stacked film containing the ZrN shell was less than that of the ratio in only SiO_2 particle-stacked film. The results reveal that these particle-stacked films exhibit a "color mixing effect" that combines specific wavelength absorption through plasmon resonance and specific wavelength diffraction owing to the periodic structure without using precious metals.

1. Introduction

Nanoparticles present a fascinating field of study, as they exist in a transitional range wherein materials exhibit both quantum and bulk properties. As particle size decreases, the bulk properties deteriorate owing to the emergence of discrete electronic states (quantum size effect) and increasing proportion of surface atoms. The characteristics exhibited by nanosizing are particularly evident in metal nanoparticles, in which unique electronic and magnetic properties have emerged, leading to novel applications in nonlinear optical switching,[1,2] catalysis,[3] and high-density information storage.[4] Similarly, semiconductor nanoparticles—commonly known as quantum dots[5]—display remarkable optical[6] and electrical[7,8] properties, attributed to the quantum confinement of electrons in a three-dimensional space.

Recently, metal nitride nanoparticles have been investigated as alternatives for optical[9], [10] and catalytic[11] functions—traditionally performed using precious metals such as Au, Ag, and Pt nanoparticles. Notably, group-four-element nitrides such as TiN, ZrN, and HfN have been reported to exhibit localized surface plasmon resonance (LSPR)[12]—a property harnessed to enhance applications in various fields. For instance, Exarhos et al. have demonstrated that the absorption wavelength of ZrN nanoparticles was tuned by coating them with silicon oxynitride.[13] ZrN–TiO_2 core-shell particles have been explored for performance enhancement in dye-sensitized solar cells.[14] ZrN–SiO_2 core-shell particles are expected to improve the efficiency of lead-free perovskite solar cells.[15] In addition, the catalytic performances of metal nitrides have been reported. In particular, ZrN nanocrystals have shown the potential to surpass the electrocatalytic efficiency of Pt in oxygen reduction reactions.[16] ZrN nanoparticles have also been examined as catalysts for methanol oxidation[17] and water-splitting reactions.[18] Thus, metal nitride nanoparticles have emerged as viable substitutes for noble metal nanoparticles, offering comparable or enhanced chemical and physical functionalities.

We focused on integrating the LSPR properties of zirconium nitride into structurally colored materials. Structurally colored materials do not change color unless their microstructure is destroyed. Thus, the interest in the use of structural color materials for coloring, in which dyes or pigments are not used, is increasing. Structural coloration of materials is achieved through multilayer film interference,[19–23] interference from fine grooves and protrusions,[24] and scattering interference caused by microscopic particles.[25,26] Research on particle-based structural color has predominantly focused on synthesizable monodisperse particles, such as polystyrene[27,28] and SiO_2.[29–31] The mechanisms for expressing structural color based on

particles can mainly be divided into colloidal photonic crystals and amorphous arrays. Colloidal photonic crystals are structures in which colloidal particles are periodically arranged. Because colloidal photonic crystals possess a complete periodic structure, they exhibit angle-dependent specific wavelength reflection due to Bragg diffraction. In contrast, amorphous arrays are structures with local periodic structures and exhibit non-iridescent structural colors without angle dependence.[32] Enhancements in contrast and scattering suppression have been achieved by incorporating black particles, such as carbon black,[33,34] polydopamine,[35] or polypyrrole.[36] Additionally, Fe_2O_3–SiO_2 core-shell particles have been developed to combine the bandgap absorption of Fe_2O_3 with reflection at specific wavelengths owing to their periodic structures.[37] Similar approaches have been reported for SiO_2–Au and SiO_2–Ag composite particles,[38,39] which utilize localized surface plasmon resonance for specific wavelength absorption in conjunction with periodic structure-based reflection, thereby providing an alternative to bandgap absorption.

However, the use of LSPR for specific wavelength absorption in structurally colored materials remains relatively unexplored, particularly without the use of precious metals. In this study, we synthesize SiO_2–core–ZrN–shell particles, where the ZrN nanoparticles exhibited LSPRs. ZrN nanoparticles were attached to SiO_2 cores using polyvinylpyrrolidone (PVP) modification, resulting in monodisperse SiO_2–ZrN core–shell particles capable of Bragg-diffracting light for structural coloration. Our findings reveal that SiO_2–ZrN core–shell particles produce a "color mixing effect," combining specific wavelength absorption through plasmon resonance and diffraction owing to periodic structures without needing precious metals.

2. Results and Discussion

2.1. Preparation and Evaluation of SiO_2–ZrN Core–Shell Particles

ZrN nanoparticles were synthesized via a solid-state metathesis reaction [22]. SiO_2 particles (150, 180, 210, 240, 270, and 300 nm) modified with polyvinylpyrrolidone-90 were mixed with the ZrN nanoparticle dispersion to obtain core–shell particles, as depicted in **Figure 1(a)**. **Figure 1(b)** shows a secondary electron (SE) scanning transmission electron microscopy (STEM) image of the obtained particles. The SE-STEM image shows that the nanoparticles are attached three-dimensionally around the large core particles. The attached nanoparticles appeared to exist as individual nanoparticles of approximately 10 nm or as aggregates with a maximum size

of approximately 30 nm. The high-angle annular dark-field (HAADF)-STEM micrograph confirmed that patches were present only on the surface of the spherical particles (Figure S1). Indeed, the contrast of the HAADF-STEM image reflects the atomic weight in brighter areas containing heavier elements, meaning that large spherical particles are surrounded by compounds containing heavier atoms than those of the core particles. The bright-field (BF)-STEM micrograph (Figure S2) shows that the nanoparticle patches were attached at the front of the spherical particles as well as at the back. **Figure 1(c)** shows the absorption spectra of the ZrN particle aqueous dispersion and the aqueous dispersions of the obtained core–shell particles containing 150, 180, 210, 240, 270, and 300 nm SiO_2 particles as cores. The aqueous dispersion of the ZrN particles exhibited maximum absorption at 705 nm, while the aqueous dispersions of the obtained particles containing 150, 180, and 210 nm SiO_2 particles showed maximum absorption at 680, 668, and 661 nm, respectively. The X-ray diffraction (XRD) profile (**Figure 1(d)**), the BF-STEM images of the obtained particles, energy-dispersive X-ray spectroscopy (EDS) mapping of the image (**Figure 1(e)**), and transmission electron microscopy (TEM) and electron diffraction images (**Figure 1(f))** revealed that the obtained particles contained ZrN as the shell. The fact that ZrN nanoparticles remained adhered to SiO_2 particles even after sample preparation for TEM, including ultrasonic dispersion in water, indicates high adhesion between the ZrN nanoparticles and SiO_2 particles. The absorption of the obtained aqueous particle dispersions containing 150 nm, 180 nm, and 210 nm (**Figure 1(c))** was attributed to ZrN nanoparticles; the obtained particles absorbed light in the 660–680 nm wavelength range through the attached ZrN nanoparticles. However, the obtained core-shell particles containing 240 nm, 270 nm, and 300 nm SiO_2 core particles and ZrN nanoparticles did not exhibit peaks in the absorption spectra because the influence of Mie scattering by SiO_2 core particles was greater than that of the absorption of ZrN particles attached to SiO_2 particles in the dispersion. The increase in particle size extends Mie scattering.[40] This results in a more significant influence of light loss due to scattering by Mie scattering than absorption by plasmon absorption to exhibit no peak in the absorption spectra using 240 nm, 270 nm, and 300 nm SiO_2 core particles.

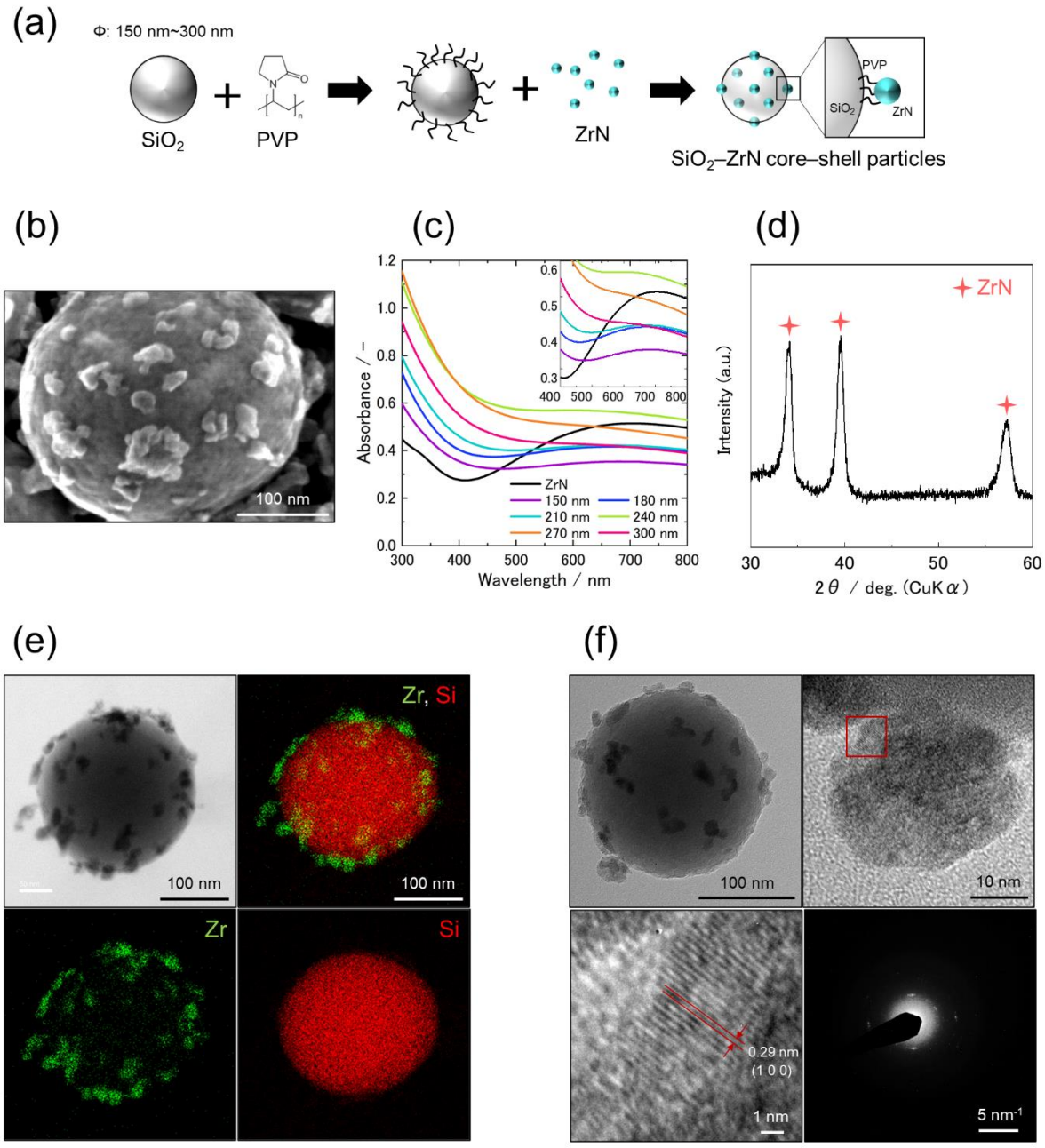

Figure 1. (a) Schematic illustration of the preparation process of SiO_2–ZrN core–shell particles. **(b)** SE-STEM image of the obtained particle. **(c)** Absorption spectra of aqueous dispersion of ZrN particles and the obtained core–shell particles containing 150, 180, 210, 240, 270, and 300 nm SiO_2 core particles. **(d)** XRD pattern of the obtained particles. **(e)** BF-STEM image of the obtained particle and EDS mapping images highlighted by elements Zr and Si. **(f)** TEM images of the obtained particle and electron diffraction image: low magnification image, intermediate magnification image, and high magnification image of the area enclosed by the red square.

2.2. Optical Properties of Core-Shell Powders and Particle-stacked Films

Figure 2 shows a photograph of the dried powder and BF-STEM images of the obtained SiO_2–ZrN core–shell particles. The BF-STEM images (Figure S3) prove that the ZrN nanoparticles were attached to the surface of the SiO_2 core particles to form SiO_2–ZrN core–shell particles. Considering that ultrasonic dispersion treatment was performed on the fabricated particles in the preparation of these particles, it can be understood that the ZrN nanoparticles and SiO_2 particles have very well adhered to each other. From the obtained particle's size distribution (Figure S4), the high monodispersion of SiO_2–ZrN core–shell particle size is evident. The powder of the obtained SiO_2–ZrN core–shell particles exhibited a color that depended on the particle size after drying at room temperature. The change in color depending on particle size indicated that the color originated from the aggregate structure of the particles.

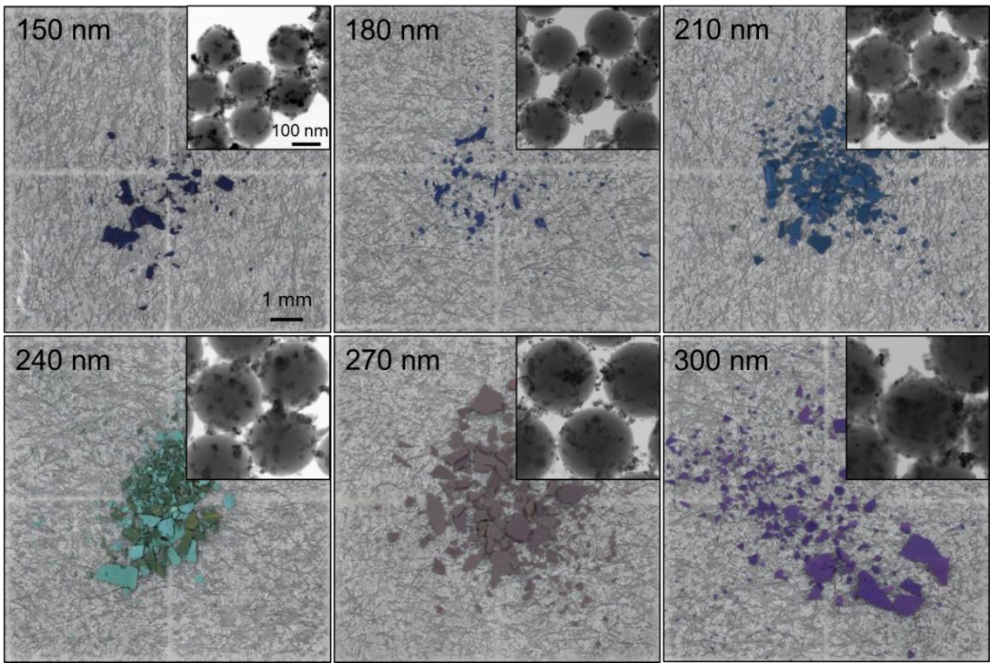

Figure 2. Photographs of the obtained powder and BF-STEM images of the SiO_2–ZrN core–shell particles containing SiO_2 core particles of 150, 180, 210, 240, 270, and 300 nm.

Particle-stacked films with SiO_2–ZrN core–shell and SiO_2 particles were fabricated by a casting method using molds to compare the effects of ZrN nanoparticles. **Figure 3(a)** shows photographs of the particle-stacked films with SiO_2–ZrN core–shell particles containing 150, 180, 210, 240, 270, and 300 nm core particles. To examine the angular dependence of the color of the particle-stacked film, images taken with the light source directed at 10° to the particle-stacked films and the camera rotated in 10° increments from 35° to 65° to the particle-stacked films are also shown. **Figure 4(a)** shows the results when SiO_2 particles were only used for

partilcle-stacked film fabrication. Regardless of whether SiO_2–ZrN core–shell particles or SiO_2 particles were used as constituent substances, the color of the particle-stacked film changed depending on the size of the constituent particles, indicating that the color of the particle-stacked films is caused by the differences in particle size.

The optical characteristics of the particle-stacked films of the obtained particles were assessed using reflection spectra. **Figure 3(b)** shows the reflection spectra of the stacked particles. In the case of the particle-stacked films containing SiO_2–ZrN core–shell particles with diameters of 150, 180, 210, 240, 270, and 300 nm, peaks were observed at 339, 385, 448, 506, 579, and 652 nm, respectively, in the reflection spectra. For the SiO_2–ZrN core–shell particles with diameters of 240, 270, and 300 nm, peaks at 314, 350, and 389 nm were observed on the short-wavelength side. The reflection of light within a photonic crystal follows Bragg's condition as follows:[32]

$$n\lambda = 2d\sin\theta$$

where n, λ, d, and θ represent the diffraction order (an integer), the wavelength of light, the lattice constant of the photonic crystal (the distance between adjacent layers), and the angle between the incident light and the normal to the layers of the photonic crystal, respectively. In amorphous arrays, the relatively broad reflection of specific wavelengths also occurs due to Bragg diffraction in the local periodic structure regions. Since the distance between layers (d) where Bragg diffraction occurs depends on the size of the particles, the wavelength (λ) of the reflected light is determined by the particle size. Therefore, the shift in the reflection peak towards longer wavelengths corresponds to an increase in the distance of the pitch in the periodic structure of the film. **Figure 4(b)** shows the reflection spectra of particle films only from SiO_2. The particle-stacked films of SiO_2 particles with diameters of 150, 180, 210, 240, 270, and 300 nm exhibited peaks at 311, 356, 427, 492, 558, and 621 nm, respectively, in the reflection spectra. Similar to the SiO_2–ZrN core–shell particles, reflection peaks appear on the short-wavelength side at 308, 337, and 369 nm when the particle sizes of the SiO_2 particle-stacked films are 240, 270, and 300 nm, respectively. In the reflection spectra of the particle-stacked films, the appearance of maxima, which shifts depending on the particle size, signifies that these maxima originate from structural colors, where periodic structures strongly reflect specific wavelengths. Although comparing the absolute value of the reflection intensity is impossible because the stacking state between the SiO_2 and ZrN core–shell particles and SiO_2 particles is not the same, a difference in the reflection spectra is observed at approximately 600 nm, corresponding to the ZrN nanoparticle absorption depending on the presence or absence of the ZrN nanoparticle shell. The reflection intensities of the particle-stacked films composed of

SiO_2–ZrN core–shell particles were lower than those of the substrate films. In contrast, the reflection intensities of the particle-stacked films composed only of SiO_2 particles were higher than that of the substrate (**Figure 4(b)**). This decrease in the reflection intensity was caused by absorption by the ZrN particles in the core.

When a structurally colored material is used as a colorant, a lower angular dependence of the visible color is desirable. Thus, the angular dependence of the reflection spectra of the particle-stacked films was evaluated. The angular dependence of the reflection spectra of the particle-stacked films composed of SiO_2–ZrN core–shell particles with core particles of 270 nm are shown in **Figure 3(c)**, and those of only SiO_2 core particles of 270 nm are shown in **Figure 4 (c)**. Comparing the reflection spectra when changing the angle, the intensity of the SiO_2 particle-stacked film (**Figure 4(c)**) was less than half that of the SiO_2–ZrN core–shell, although the reflection intensities of the SiO_2 particles were the same or higher than those of the SiO_2–ZrN core–shell when measured with an integrating sphere unit. Furthermore, when the angle changed from 35° to 65°, the maximum peak wavelength changed by 14 nm for the particle-stacked films composed of SiO_2–ZrN core–shell particles and 28 nm for the particle-stacked films consisting of only SiO_2 particles. Even in the case of particle-stacked films with 240 and 300 nm particles, where peaks could be detected when the angle was changed, it was found that, similar to the results with 270 nm particles, the shift was smaller for SiO_2–ZrN core–shell particles (Figure S5, Figure S6). These results suggest that the SiO_2–ZrN core–shell particles are stacked more randomly than the SiO_2 particles. The difference in the peak wavelength shift of the reflection spectrum between the SiO_2 and ZrN core–shell particle-stacked film and SiO_2 particle-stacked film when the angle was altered by 30° was 14 nm, imperceptible to the naked eye. However, this result quantitatively demonstrates that the core–shell particle-layered film exhibits less angular dependence than the silica particle-layered film.

The stacked particle films were observed using field-emission scanning electron microscopy (FE-SEM) to investigate the stacking state of the particles. **Figure 3(d, e)** shows surface and cross-sectional FE-SEM images of the particle-stacked films. The surfaces of the particle-stacked films composed of SiO_2–ZrN core–shell particles were smoother than those of the SiO_2 particle-stacked films (Figure S7) because the particle-stacked films composed of SiO_2–ZrN core–shell particles had fewer irregularities made up of particle agglomerates than SiO_2, thus reflecting the differences in the state of particle film formation. Although no noticeable difference was observed in the surface images of the particle-stacked films at medium

magnification, differences between the particle-stacked films composed of SiO_2–ZrN core–shell particles and SiO_2 particles were visible in the surface FE-SEM images at high magnification. Only spherical particles were observed in the SiO_2 particle stack (Figure S8), whereas protrusions on the particle surface were observed in the SiO_2–ZrN core-shell particles. These protrusions correspond to ZrN nanoparticles attached to SiO_2 core particles. The Fourier transform image of the surface of the SiO_2 particle-stacked film clearly exhibits rings derived from the periodic structure compared to the image of the surface of the particle-stacked film of SiO_2–ZrN core-shell particles. More distinct rings indicate higher periodicity of the constituent particles. Thus, the periodicity of the SiO_2–ZrN core-shell particles in the particle-stacked films is lower than that of the SiO_2 particle-stacked films, implying that the particle-stacked films of the SiO_2–ZrN core-shell particles have less angular dependence on reflection, consistent with the reflection spectrum results (**Figure 3(c)**). From the cross-sectional FE-SEM images (**Figure 3(e)**), no significant periodicity was observed in the height direction for both the particle-stacked films of the SiO_2–ZrN core-shell particles and SiO_2 particles (Figure S9). It is considered that there is no significant difference in the monodispersity of the particle size distribution (Figure S4) and no major differences are observed in the stacked state for each particle size. In this study, amorphous arrays were obtained. If a regularly arranged 3D SiO_2–ZrN core–shell microsphere photonic crystal is obtained, the peak in the reflection spectrum becomes narrower and the reflectance increases due to the regular arrangement, resulting in a relatively lower effect of plasmon absorption by the ZrN shell. Consequently, the influence of color based on reflection from the photonic crystals becomes more significant. The angle dependence of a photonic crystal is expected to be greater than that of the amorphous array obtained in this study.

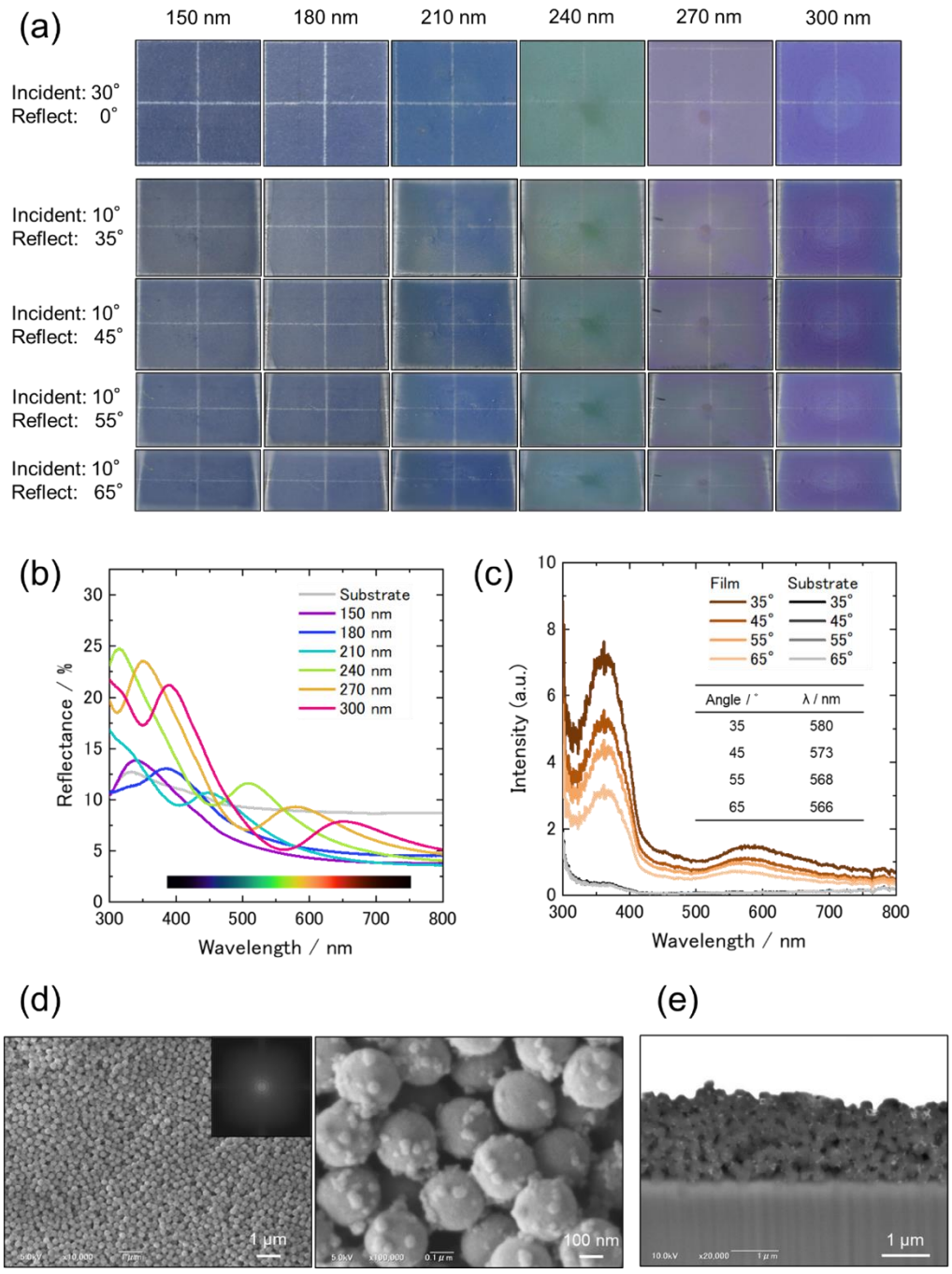

Figure 3. (a) Photographs of the particle-stacked films comprising SiO_2–ZrN core–shell particles with SiO_2 core particles of 150, 180, 210, 240, 270, and 300 nm. These films were photographed on 5 mm graph paper; the cross lines in the images are grid lines of the background paper. The images show an area of 10 mm in length and 10 mm in width of the particle-stacked films. **(b)** Reflection spectra of the particle-stacked films composed of SiO_2–ZrN core–shell particles with core particles of 150–300 nm. The light was incident at 5° from the vertical plane of the particle laminated film, with the reflected light detected with an integrating sphere unit. **(c)** Angular dependence of reflection spectra of particle-stacked films comprising SiO_2–ZrN core–shell particles with core particles of 270 nm. The reflectance intensity was measured to analyze angular dependence: the incident angle of the light source to the particle-stacked film was 10°, and the reflection angle to the detector was in 10° increments from 35° to 65°. **(d)** Surface FE-SEM images of particle-stacked films comprising SiO_2–ZrN core–shell particles with core particles of 270 nm and Fourier transform image. **(e)** Cross-sectional FE-SEM images of particle-stacked films comprising SiO_2–ZrN core–shell particles with core particles of 270 nm.

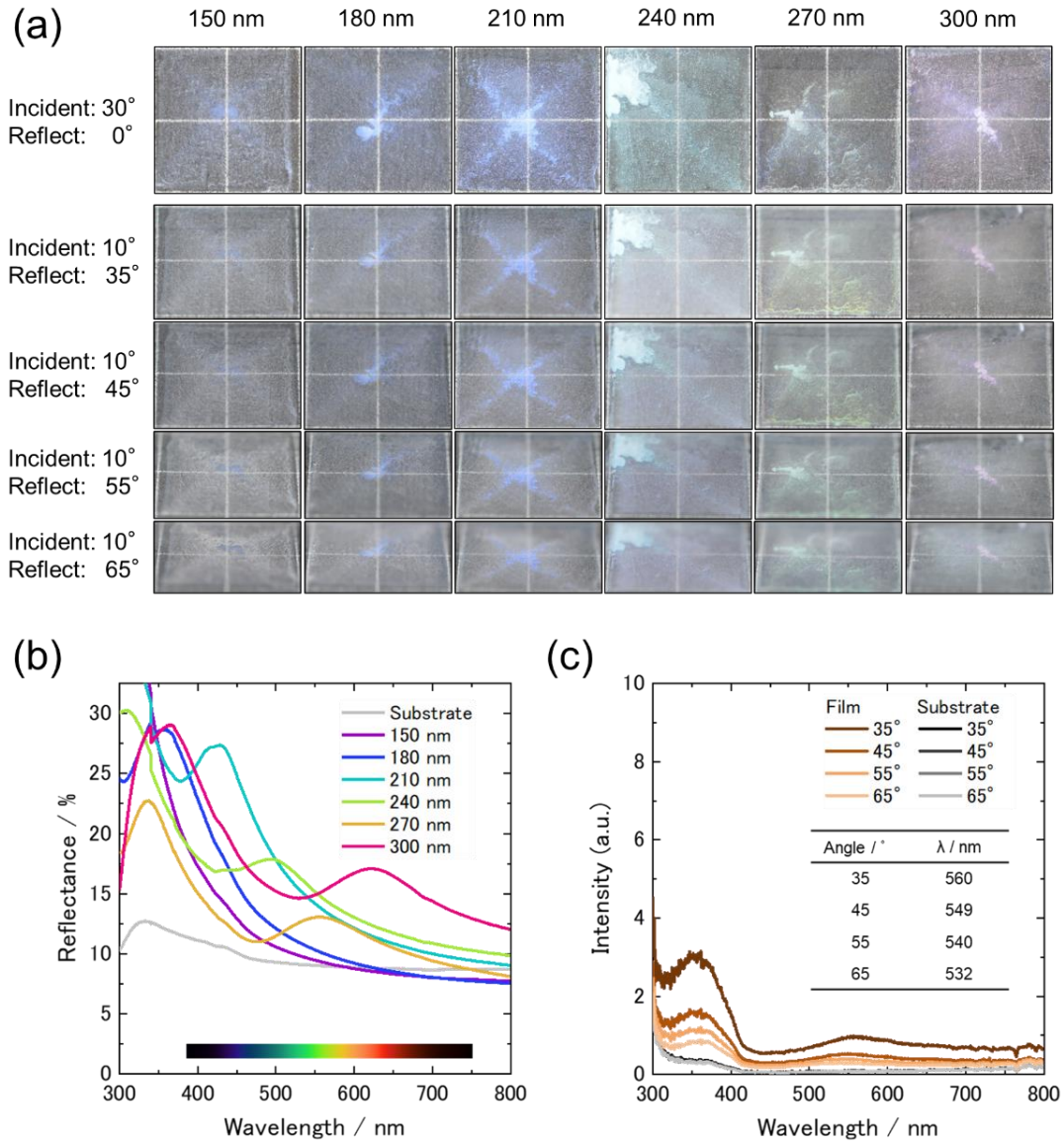

Figure 4. (a) Photographs of the particle-stacked film comprising SiO_2 particles with diameters of 150, 180, 210, 240, 270, and 300 nm. These films were photographed on 5 mm graph paper; the cross lines in the images are grid lines of the background paper. The images show an area of 10 mm in length and 10 mm in width of the particle-stacked films. **(b)** Reflection spectra of the particle-stacked films composed of SiO_2 particles with diameters of 150–300 nm. The light was incident at 5° from the vertical plane of the particle laminated film, with the reflected light detected with an integrating sphere unit. **(c)** Angular dependence of reflection spectra of the particle-stacked films of SiO_2 particles with diameters of 270 nm. The reflectance intensity was measured to analyze angular dependence: the incident angle of the light source to the particle-stacked film was 10°, and the reflection angle to the detector was in 10° increments from 35° to 65°.

Table 1 lists the maximum peaks, reflectance, and reflection intensity ratio ($R_l\ R_s^{-1}$) of the long-wavelength side (R_l) to the reflection intensity on the short-wavelength (R_s) side in the reflection spectra of particle-stacked films using SiO_2–ZrN core–shell particles and SiO_2 particles. When comparing identical SiO_2 core particle sizes, the wavelength of the peak in the reflection spectrum of the SiO_2–ZrN core–shell particles shifted to longer wavelengths than that of the SiO_2 particles because the attachment of the ZrN particles increased the total particle size and widened the periodic interval. The reflection intensity ratio ($R_l\ R_s^{-1}$) of the particle-stacked films using SiO_2 particles is almost constant at 0.57–0.59 when the particle size is between 240 nm and 300 nm, while the ratio of SiO_2–ZrN core–shell particles decreases from 0.47 to 0.37. The prepared ZrN nanoparticles absorb across the entire reflection band with a peak at 700 nm because the prepared ZrN nanoparticles are not completely uniform in size. As shown in **Figure 1c**, the ZrN nanoparticles used in the shell exhibit a broad absorption spectrum with a peak at 700 nm. Therefore, it is considered that the fabricated SiO_2–ZrN core–shell particles also absorb across the entire reflection band with a peak at 700 nm. The reflection intensity of the particle-stacked films using SiO_2–ZrN core–shell particles decreased as the reflection wavelength on the long-wavelength side approached 660–680 nm, corresponding to the absorption of ZrN, thus indicating that the reflection of particle-stacked films using SiO_2–ZrN core–shell particles is suppressed by the LSPR absorption of ZrN owing to the presence of ZrN particles around SiO_2. Particle-stacked films of SiO_2–ZrN core–shell particles with a high distribution density of ZrN nanoparticles (Figure S10), prepared by attaching ZrN nanoparticles to PVP-modified SiO_2 particles without washing, exhibited a more pronounced color mixing effect (Figure S11, Table S1). This suggests that the color mixing effect can be tuned by the distribution density of ZrN nanoparticles in the shell. In addition, similar to how the peak of the reflection spectrum shifted with changes in the size of the core particles, a change in the shell thickness of core-shell particles is expected to change the pitch of the periodic structure within the particle-stacked films, which may result in a shift in the peak wavelength of the reflectance spectrum.

We can conclude that the synthesized core-shell particle stacked film exhibits the "color mixing effect" that combines structural color derived from the periodic structure and specific wavelength absorption owing to LSPR. Hence, SiO_2–ZrN core–shell particles offer the potential to be effective optical materials for tuning reflection and absorption spectra owing to the combination of LSPR and the periodic structure of composites without precious metals.

Table 1. Particle size (φ), wavelength of maximum peaks (λ), reflectance (*R*), and reflection intensity ratio (R_l R_s^{-1}) of the long wavelength side (R_l) to the reflection intensity on the short wavelength (R_s) side in the reflection spectrum of the particle-stacked films using SiO_2–ZrN core–shell particles and SiO_2 particles.

Type	Φ / nm (core size)	λ / nm	*R* / %	R_l R_s^{-1} / –
SiO_2–ZrN core–shell particles	150	339	13.84	–
	180	385	13.05	–
	210	448	10.67	–
	240	314, 509	24.77, 11.63	0.47
	270	350, 579	23.55, 9.32	0.40
	300	389, 652	21.21, 7.88	0.37
SiO_2 particles	150	311	40.09	–
	180	356	28.74	–
	210	427	27.37	–
	240	306, 485	31.31, 18.07	0.58
	270	337, 558	22. 74, 13.05	0.57
	300	369, 621	28.98, 17.10	0.59

3. Conclusion

We successfully prepared SiO_2–ZrN core–shell particles. Color-controllable structural color materials can be obtained by combining the LSPR of ZrN nanoparticles around SiO_2 core particles and the diffraction properties of periodic structures. The ZrN nanoparticles attached to the SiO_2 core absorb the light around 700 nm to exhibit reflection spectra with a "color mixing effect" that combines specific wavelength absorption through plasmon resonance and specific wavelength diffraction owing to the periodic structure. The change in the particle size enabled a shift in the structural color reflection, with the intensity of the reflection controlled by the particles as shell components. We believe that the SiO_2–ZrN core–shell particles offer the potential to be effective optical materials for tuning the reflection and absorption spectra, owing to the combination of LSPR and the periodic structure of the composites without precious metals.

4. Experimental Section

Materials:

Zirconium dioxide (ZrO_2, 10 nm) was purchased from ITEC Co., Ltd. Magnesium nitride (Mg_3N_2) was purchased from Sigma Aldrich. SiO_2 particles were purchased from FUJI CHEMICAL Co., Ltd. Polyvinylpyrrolidone (PVP, K 90 Average Molecular weight. 360000)

was purchased from TOKYO CHEMICAL INDUSTRY Co., Ltd. Hydrochloric acid (1 M) was purchased from KANTO CHEMICAL Co., Inc.

Sample preparation:

ZrN nanoparticle dispersion

ZrN nanoparticles were synthesized using a modified version of the process described in our previous report. A mixture of 1 g of zirconium dioxide nanopowder and a three-molar excess Mg_3N_2 powder was mixed for 5 min in an Ar glove box using an agate mortar. The resulting mixture was transferred to an alumina combustion boat and hermetically sealed in a plastic bag using a zip. The powder confined in the plastic bag was immediately inserted into a quartz tube and heated at 1000 °C for 12 h under nitrogen gas flow in a tubular furnace. After natural cooling to room temperature, 0.2 g of the final product was transferred to a beaker and mixed with 25 mL of 1.0 M HCl solution. The mixture was sonicated for 20 min, and water (20 mL) was added. After stirring for 1 h, the supernatant was separated by centrifugation for 1 h at 11000 rpm. The residual precipitate was redispersed in 5 mL of water by sonication and centrifuged for 15 min at 3300 rpm. The blue supernatant was collected to obtain a dispersion of the ZrN nanoparticles.

SiO_2–ZrN core–shell particles

PVP 90 (0.1 g) was added to a water dispersion (50 mL) of SiO_2 particles (0.05 g) while stirring at 400 rpm. The mixture was continuously stirred for one night. Subsequently, the liquids were centrifuged at 3300 rpm for 15 min, with the supernatant discarded to remove the solution containing unattached PVP 90. The precipitate was resuspended in water (50 mL) and sonicated. The suspended liquid was centrifuged again at 3300 rpm for 15 min, with the supernatant discarded again. The residue was suspended in water (5 mL) to obtain SiO_2 particles modified with PVP 90. The ZrN dispersion (0.4 mL) was added to a 1 mL dispersion of modified SiO_2 particles. The mixture was then shaken and sonicated. The obtained dispersion was centrifuged at 3300 rpm for 15 min, with the supernatant discarded to remove the ZrN nanoparticles not attached to the SiO_2 particles. The residual precipitate was dried to obtain the SiO_2–ZrN core–shell particles.

Particle-stacked films

The obtained SiO_2–ZrN core–shell and SiO_2 particles were arrayed onto glass substrates by drop-casting using silicone molds. Silicone molds, with a thickness of 3 mm and a 1 cm square hole, were pressed onto glass substrates and pasted. Nanoparticles' dispersion (0.1 wt.%, 0.3 mL) was cast into the hole of the silicon mold. After natural drying for one day, water as a dispersion medium was evaporated, and the particles self-assembled to form a particle-stacked film.

Material Characterization:

X-ray Diffraction (XRD)

The crystalline phase was analyzed using an X-ray diffraction (XRD) diffractometer (Cu Ka, Mini-Flex 600, Rigaku, Japan). The diffraction angle 2θ was scanned in the range of 30–60° at a rate of 5° min^{-1}.

Transmission Electron Microscopy (TEM)

The morphologies of the core–shell particles were evaluated using TEM (JEM-2010, JEOL, Japan), with the dispersion of the core–shell particles drop-cast onto copper-mesh TEM grids. The acceleration voltage of the electron gun used for the observation was 200 kV.

Scanning Transmission Electron Microscopy (STEM)

The morphology of the core–shell particles was examined using scanning transmission electron microscopy (STEM) with an HD-2000 instrument (HITACHI, Japan). The sample was prepared following the same procedure as that for the TEM observation, with the electron gun acceleration voltage set to 200 kV. Energy-dispersive X-ray spectroscopy (EDS) was performed using the same equipment to investigate the elemental distributions of the particles.

Field Emission Scanning Electron Microscope (FE-SEM)

The surface and cross-sectional morphologies of the particle-stacked films were observed using field-emission scanning electron microscopy (FE-SEM) with a JIB–4601F instrument (JEOL, Japan). The particle-stacked films were observed at an electron gun acceleration voltage of 200 kV after the films were coated with platinum. The observed cross-section was formed by the radiation of a focused ion beam onto the surface of the tungsten-coated particle-stacked film.

Spectrum measurement

The UV-Vis absorption spectra of the SiO_2–ZrN core–shell particle dispersions were recorded using a V-700 spectrometer (JASCO, Japan). The dispersion was then placed in a 1 cm square quartz cell and mounted on a holder for measurement. Water was used as the background for the absorbance measurements. The scanning rate was 200 nm min^{-1} and the bandwidth was 2 nm, with a range of wavelengths scanned from 300 nm to 800 nm. The reflection spectra of the particle-stacked films were measured using the same instrument equipped with an integrating spherical unit. The particle-stacked films were placed on a holder for measurement; the scanning rate was 200 nm min^{-1}, with a bandwidth of 5 nm and a range of wavelengths scanned from 300 nm to 800 nm. The reflectance intensity was measured to analyze the angular dependence. Variable-angle reflection measurement optics, C10027A10687 (Hamamatsu Photonics, Japan) were used to expose the particle-stacked films to white light and detect the reflected light. A xenon lamp was used as the light source to measure the reflection spectra. A photonic multichannel analyzer C10027 (Hamamatsu Photonics, Japan) was used to analyze the detected signals. The incident angle of the light source to the particle-stacked film was 10°, with the reflection angle to the detector varied in 10° increments from 35° to 65°.

Supporting Information

Supporting Information is available from the Wiley Online Library or from the author.

Acknowledgments

Shinji Noguchi thanks Hokkaido University "Ambitious Leader's Program (ALP)" supported by the Ministry of Education, Culture, Sports, Science and Technology (MEXT), Japan. This research was financially supported by JST SPRING (Grant Number JPMJSP2119) from the Japan Science and Technology and Agency (JST) and a Grant-in-Aid for JSPS Fellows (No. 23KJ0014) from the Japan Society for the Promotion of Science (JSPS). This work was supported by the "Advanced Research Infrastructure for Materials and Nanotechnology in Japan (ARIM)" of the MEXT. Grant Number JPMXP1223HK0087 (Hokkaido University). Shinji Noguchi is grateful to Dr. Yuko Mori, Dr. Naomi Hirai, Dr. Atsuki Sawa, and Dr. Wang of Hokkaido University for their support in electron microscopy analysis.

Received: (January 30, 2024)
Revised: (March 17, 2024)
Published online: (April 15, 2024)

References

[1] X. Gao, C. Zou, H. Zhou, C. Yuan, J. He, X. Luo, *J. Alloys. Compd.* **2020**, *819*, DOI: 10.1016/j.jallcom.2019.153003.

[2] X. Liu, *Front. Mater.* **2018**, *5*, DOI: 10.3389/fmats.2018.00059.

[3] X. Wang, Z. Yang, Y. Zhang, L. Jing, Y. Zhao, Y. Yan, K. Sun, *Fuel Cells* **2014**, *14*, 35, DOI: 10.1002/fuce.201300102.

[4] S. Liu, S. Fu, X. Zhang, X. Wang, L. Kang, X. Han, X. Chen, J. Wu, Y. Liu, *Opt. Mater. Express.* **2018**, *8*, 1143, DOI: 10.1364/ome.8.001143.

[5] A. L. Efros, L. E. Brus, *ACS Nano* **2021**, *15*, 6192, DOI: 10.1021/acsnano.1c01399.

[6] F. Liu, M. H. Jang, H. D. Ha, J. H. Kim, Y. H. Cho, T. S. Seo, *Advanced Materials* **2013**, *25*, 3657, DOI: 10.1002/adma.201300233.

[7] M. Henini, A. Patane Á, A. Polimeni, A. Levin, L. Eaves, P. C. Main, G. Hill, *Microelectronics J.* **2002**, *33*, 313, DOI: 10.1016/S0026-2692(01)00124-0.

[8] Z. J. Horva Âth, L. Do Âzsa, V. Van Tuyen, B. Po, Í. Èr, A. Â. Nemcsics, P. Frigeri, E. Gombia, R. Mosca, S. Franchi, *Thin Solid Films* **2000**, *367*, 89, DOI: 10.1016/S0040-6090(00)00701-X.

[9] U. Guler, V. M. Shalaev, A. Boltasseva, *Materials Today* **2015**, *18*, 227, DOI: 10.1016/j.mattod.2014.10.039.

[10] K. L. Kelly, E. Coronado, L. L. Zhao, G. C. Schatz, *Journal of Physical Chemistry B* **2003**, *107*, 668, DOI: 10.1021/jp026731y.

[11] C. G. Freyschlag, R. J. Madix, *Materials Today* **2011**, *14*, 134, DOI: 10.1016/S1369-7021(11)70085-2.

[12] R. A. Karaballi, G. Humagain, B. R. A. Fleischman, M. Dasog, R. A. Karaballi, G. Humagain, B. R. A. Fleischman, P. R. M. Dasog, *Angewandte Chemie* **2019**, *58*, 3 DOI: 10.1002/ange.201813134.

[13] S. Exarhos, A. Alvarez-Barragan, E. Aytan, A. A. Balandin, L. Mangolini, *ACS Energy Letter* **2018**, *3*, 2349, DOI: 10.1021/acsenergylett.8b01478.

[14] Y. Di, T. Qin, *Opt. Mater.* **2022**, *132*, DOI: 10.1016/j.optmat.2022.112813.

[15] A. A. Mohsen, M. Zahran, S. E. D. Habib, N. K. Allam, *Sci. Rep.* **2020**, *10*, DOI: 10.1038/s41598-020-63745-7.

[16] Y. Yuan, J. Wang, S. Adimi, H. Shen, T. Thomas, R. Ma, J. P. Attfield, M. Yang, *Nat. Mater.* **2019**, *19*, 282, DOI: 10.1038/s41563-019-0535-9.

[17] O. A. Baturina, A. Epshteyn, A. C. Leff, A. P. Purdy, T. Brintlinger, B. S. Simpkins, E. Y. Santiago, A. O. Govorov, *J. Electrochem. Soc.* **2021**, *168*, 016503, DOI: 10.1149/1945-7111/abd605.

[18] Y. Liu, X. Zhang, L. Lu, J. Ye, J. Wang, X. Li, X. Bai, W. Wang, *Chinese Chemical Letters* **2022**, *33*, 1271, DOI: 10.1016/j.cclet.2021.07.054.

[19] M. A. Haque, G. Kamita, T. Kurokawa, K. Tsujii, J. P. Gong, *Advanced Materials* **2010**, *22*, 5110, DOI: 10.1002/adma.201002509.

[20] M. A. Haque, T. Kurokawa, G. Kamita, Y. Yue, J. Ping Gong, *Chemistry of Materials* **2011**, *23*, 5200, DOI: 10.1021/cm2021142.

[21] Y. Yue, T. Kurokawa, A. Haque, T. Nakajima, T. Nonoyama, X. Li, I. Kajiwara, J. P. Gong, *Nat. Commun.* **2014**, *5*, 4659, DOI: 10.1038/ncomms5659.

[22] M. Lama, J. Ping Gong, *ACS Omega* **2023**, *8*, 25185, DOI: 10.1021/acsomega.3c02274.

[23] C. Kyungjae Chung, S. Yu, C.-J. Heo, J. Won Shim, S.-M. Yang, M. Gyu Han, H.-S. Lee, Y. Jin, S. Yoon Lee, N. Park, J. H. Shin, K. Chung, J. H. Shin, S. Yu, N. Park, C. Heo, J. W. Shim, S. Yang, M. G. Han, H. Lee, Y. Jin, S. Y. Lee, *Adv. Mater.* **2012**, *24*, 2375, DOI: 10.1002/adma.201200521.

[24] A. Saito, K. Ishibashi, J. Ohga, Y. Hirai, Y. Kuwahara, *Journal of Photopolymer Science and Technology* **2018**, *31*, 113, DOI: 10.2494/photopolymer.31.113.
[25] J. He, S. Liu, G. Gao, M. Sakai, M. Hara, Y. Nakamura, H. Kishida, T. Seki, Y. Takeoka, *Adv. Opt. Mater.* **2023**, *11*, DOI: 10.1002/adom.202300296.
[26] K. Ohno, Y. Mizuta, *ACS Appl. Polym. Mater.* **2019**, *2*, 368, DOI: 10.1021/acsapm.9b00839.
[27] X. Zhu, T. Wei, M. D. Shawkey, T. Xing, G. Chen, *Ind. Crops. Prod.* **2022**, *176*, DOI: 10.1016/j.indcrop.2021.114419.
[28] L. Schertel, L. Siedentop, J. M. Meijer, P. Keim, C. M. Aegerter, G. J. Aubry, G. Maret, *Adv. Opt. Mater.* **2019**, *7*, DOI: 10.1002/adom.201900442.
[29] D. S. Choi, J. H. Choi, C. Y. Lee, *Applied Sciences* **2020**, *10*, DOI: 10.3390/app10010420.
[30] L. Abraham, T. Thomas, M. Pichumani, *Chem. Phys.* **2022**, *563*, DOI: 10.1016/j.chemphys.2022.111682.
[31] W. Gao, M. Rigout, H. Owens, *Appl. Surf. Sci.* **2016**, *380*, 12, DOI: 10.1016/j.apsusc.2016.02.106.
[32] Y. Hu, Y. Zhang, D. Yang, D. Ma, S. Huang, *Mater. Adv.* **2021**, *2*, 6499, DOI: 10.1039/d1ma00477h.
[33] B. Liu, J. Fan, W. Liu, G. Zhang, Z. Wu, *Dyes and Pigments* **2022**, *208*, DOI: 10.1016/j.dyepig.2022.110810.
[34] M. Sakai, H. Kim, Y. Arai, T. Teratani, Y. Kawai, Y. Kuwahara, K. Abe, Y. Kuwana, K. Ikeda, K. Yamada, Y. Takeoka, *ACS Appl. Nano. Mater.* **2020**, *3*, 7047 DOI: 10.1021/acsanm.0c01366.
[35] M. Xiao, Y. Li, M. C. Allen, D. D. Deheyn, X. Yue, J. Zhao, N. C. Gianneschi, M. D. Shawkey, A. Dhinojwala, *ACS Nano* **2015**, *9*, 5454, DOI: 10.1021/acsnano.5b01298.
[36] X. Yang, D. Ge, G. Wu, Z. Liao, S. Yang, *ACS Applied Materials & Interfaces* **2016**, *8*, 16289, DOI: 10.1021/acsami.6b03739.
[37] J. Han, E. Lee, J. K. Dudoff, M. Bagge-Hansen, J. R. I. Lee, A. J. Pascall, J. D. Kuntz, T. M. Willey, M. A. Worsley, T. Y. J. Han, *Adv. Opt. Mater.* **2017**, *5*, DOI: 10.1002/adom.201600838.
[38] T. Ung, L. M. Liz-Marzán, P. Mulvaney, *Colloids. Surf. A. Physicochem. Eng. Asp.* **2002**, *202*, 119, DOI: 10.1016/S0927-7757(01)01083-4.
[39] W. Wang, S. A. Asher, *J. Am. Chem. Soc.* **2001**, *123*, 12528, DOI: 10.1021/ja011262j.
[40] G. Mie, *Ann. Phys.* **1908**, *330*, 377-445, DOI:10.1002/andp.19083300302.

Table of contents

Structural color materials with a color mixing effect using SiO_2–ZrN core–shell particles, where ZrN nanoparticles used as shell exhibited localized surface plasmon resonance, were developed. The particle-stacked films can be a material that exhibits a "color mixing effect" that combines specific wavelength absorption through plasmon resonance and specific wavelength diffraction by the periodic structure without using precious metals.

S. Noguchi, M. Lama, Y. Fujii, A. Miura, K. Tadanaga*

Structural Color Materials with Color Mixing Effect Using Noble Metal-free Plasmonic Particles in ZrN–SiO_2 System

ToC figure

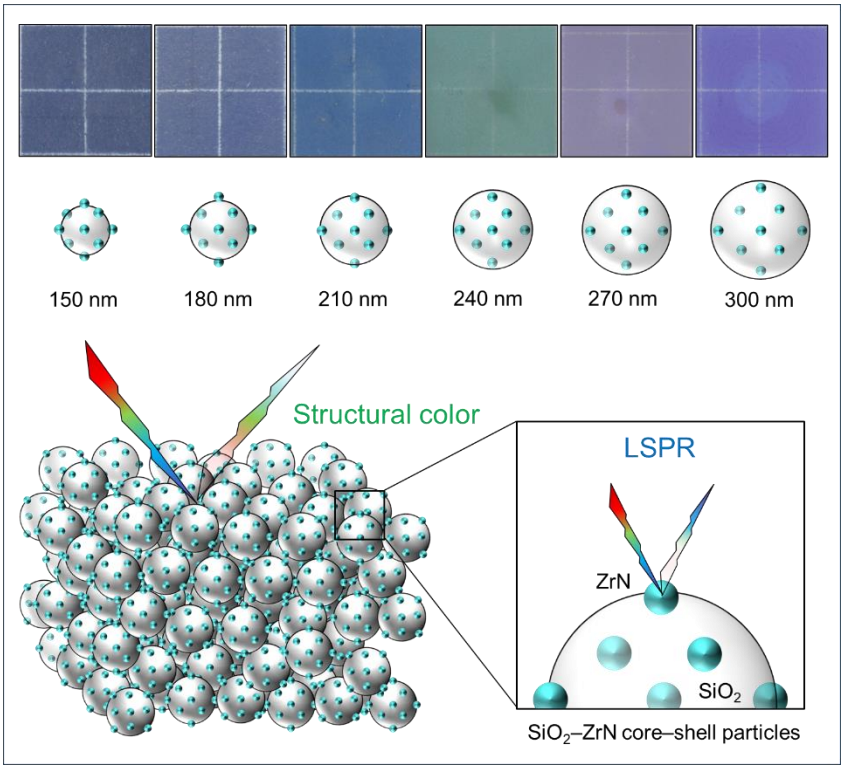

AUTHOR INFORMATION

Corresponding Author

Kiyoharu Tadanaga

[3]Faculty of Engineering, Hokkaido University, Kita-13, Nishi-8, Kita-ku, Sapporo 060-8628, Japan; ORCID: https://orcid.org/0000-0002-3319-4353; Email: tadanaga@eng.hokudai.ac.jp

Author

Shinji Noguchi

[1]Graduate School of Chemical Sciences and Engineering, Hokkaido University, Kita-13, Nishi-8, Kita-ku, Sapporo 060-8628, Japan; ORCID: https://orcid.org/0000-0003-1546-9998; Email: shinji@eis.hokudai.ac.jp

Milena Lama

[2]Institute for Chemical Reaction Design and Discovery (WPI-ICReDD), Hokkaido University, Kita-21, Nishi-11, Kita-ku, Sapporo 001-0021, Japan; ORCID: https://orcid.org/0000-0001-8373-6336; Email: lama@icredd.hokudai.ac.jp

Yuta Fujii

[3]Faculty of Engineering, Hokkaido University, Kita-13, Nishi-8, Kita-ku, Sapporo 060-8628, Japan; ORCID: https://orcid.org/0000-0002-8381-4119; Email: fujii.yuta@eng.hokudai.ac.jp

Akira Miura

[3]Faculty of Engineering, Hokkaido University, Kita-13, Nishi-8, Kita-ku, Sapporo 060-8628, Japan; ORCID: https://orcid.org/0000-0003-0388-9696; Email: amiura@eng.hokudai.ac.jp

Author Contributions

- Shinji Noguchi led the study, including conceiving the study idea, developing the experimental plan, conducting the experiments, drafting the original manuscript, and securing some research funding.
- Milena Lama assisted in developing the experimental plan and conducted some of the experiments.
- Yuta Fujii discussed the results.
- Akira Miura discussed the results.
- Kiyoharu Tadanaga played a multifaceted role, including conceiving the study idea, developing the experimental plan, securing a portion of the research funding, and overseeing the entire study's execution.

All authors reviewed the manuscript draft and revised it critically on intellectual content. All authors approved the final version of the manuscript to be published.

Funding Source

- Hokkaido University "Ambitious Leader's Program" supported by the Ministry of Education, Culture, Sports, Science and Technology (MEXT), Japan
- JST SPRING (Grant Number JPMJSP2119) from the Japan Science and Technology and Agency (JST)
- Grant-in-Aid for JSPS Fellows (No. 23KJ0014) from the Japan Society for the Promotion of Science (JSPS)
- Advanced Research Infrastructure for Materials and Nanotechnology in Japan (ARIM)" of the MEXT. Grant Number JPMXP1223HK0087 (Hokkaido University)

Notes

The authors declare no competing financial interests.